Vehicle Following Control with Improved Information Flow Using Two-Vehicle-Look-Ahead-Plus-Rear-Vehicle Topology

Mu'azu Jibrin Musa ⓘ**, Shahdan Sudin, Zaharuddin Mohamed, Abubakar Abisetu Oremeyi, Yahaya Otuoze Salihu** ⓘ**, and Gambo Danasabe** ⓘ

Abstract There exists an inherent trade-off among vehicle following performance indices (position, speed, acceleration and jerk) of any vehicle following system. The use of unrealistic information flow topology (IFT) affects the overall performance of a convoy. This chapter proposes an improved IFT of the two-vehicle look-ahead-plus-rear-vehicle control, which aimed to mitigate the trade-off with a wider range of control regions and to provide acceptable performance simultaneously. The proposed improved topology has explored the single vehicle's dynamic equations and derived the external uncertainties which are modeled together as a unit. The vehicle model is then integrated into the control strategy in order to improve the performance of the convoy. Changes in parameters of the improved convoy are compared with the most widely used conventional convoy topologies (one-vehicle look-ahead and the two-vehicle look-ahead). The results showed that the proposed following vehicle control topology has improved performance of an increase in the inter-vehicular spacing by 19.45 and 18.20%, reduce in both acceleration and jerk by 20.28, 15.17,

M. J. Musa (✉) · S. Sudin · Z. Mohamed
Division of Control and Mechatronics Engineering, Universiti Teknologi Malaysia, Johor Bahru, Malaysia
e-mail: mmjibrin@utm.my

S. Sudin
e-mail: shahdan@utm.my

Z. Mohamed
e-mail: zahar@utm.my

A. A. Oremeyi
School of Engineering, Kogi State Polytechnic Lokoja, Itakpe Campus, Nigeria
e-mail: abubakarabisetu@kogipolytechnic.edu.ng

Y. O. Salihu
Department of Computer Engineering, Kaduna Polytechnic, Zaria, Nigeria
e-mail: s.otuoze@kadunapolytechnic.edu.my

G. Danasabe
Department of Electrical and Electronics Engineering Technology, School of Engineering Technology, Nuhu Bamalli Polytechnic, Zaria, Kaduna, Nigeria
e-mail: danasabegambo@gmail.com

261

25.09 and 6.25% as against the conventional, respectively. This signifies that the proposed vehicle follower will always remain in between the rear-vehicle and the predecessor-vehicle for safety, and it also gave more ride comfort due to the achieved low acceleration and jerk in the following vehicle.

Keywords Following topology · Passenger's comfort · Road vehicle · Vehicle dynamics · Vehicle safety

1 Introduction

Rise in population in urban areas resulted in high demand for highway travel. So building of more highways to meet with this challenge is never the solution to this growth in traffic density. It was projected that transportation of goods alone will almost double by 2020 as compared to 2012. The traffic problem is not only a main problem of the metropolis, but it is also common in small urban and rural areas [1].

The deployment of self-driving vehicles on the highway has the potential of playing important role in intelligent traffic systems by minimizing the issues associated with traffic congestion, facilitating people's safety, reducing energy wastage, maximizing ride comfort and cutting down fuel consumption [2]. Several vehicle convoy models and controllers were proposed in the literature [3, 4]. Vehicle control strategies need vehicles in the same convoy to move at a stable agreement in speed while maintaining the desired inter-vehicular spacing with respect to the neighboring vehicles within the convoy. Furthermore, it has to ensure stable string which is the ability of the controlled vehicle to move along the convoy without amplifying the oscillation of the leading vehicle upstream and also to provide minimum jerk in the control vehicle [2].

To achieve string stability, desired inter-vehicular spacing and ride comfort, the vehicle convoy must comply with either of the control policies, the variable spacing or the constant spacing. It is of importance to know that ride comfort is the third-order differential of the displacement of the vehicle, which is called as the jerk of the vehicle. In the variable spacing policy, the inter-vehicle spacing is large (a function of velocity), which is applicable for low traffic density conditions. This technique facilitates string stability using onboard information. This implies that vehicles do not rely largely on information from other vehicles. While constant spacing policy depends mostly on inter-vehicle communication, this policy facilitates string stability with little spacing and it is generally applicable in high traffic density conditions [2]. To achieve desired spacing, the time headway would play a significant role [5] in inter-vehicular spacing and to avoid collision with the vehicles of the convoy. The constant time headway (CTH) describes the desired inter-vehicular spacing is proportional to the control vehicle's speed, and the constant of proportionality from the CTH policy is referred to as the time headway (h) [6, 7]. To achieve the passenger's comfort, the control vehicle's jerk must be minimized to not more than one-third of the vehicle's acceleration (not more than 5 ms^{-3}) [8, 9]. The smaller the vehicle's jerk, the more comfortable are the passengers in the vehicle [10].

String stability is mostly achieved in situations where errors (spacing and information flow) are not amplified within the convoy as vehicles move. For the perfect cancellation of such errors, the errors must have the same sign so as to avoid collision within the convoy [11–13]. The concept of vehicle convoy refers to a string of vehicles that aims to keep a specified, but not necessarily constant inter-vehicle distance with respect to either of the two policies discussed above.

Researchers have been working in the area of vehicle convoy topology control with the aim to come up with the optimum topology, which will give an improved controlled vehicle communication, string stability, chattering free and maximize passengers comfort. Dunbar and Caveney [14] modeled the limited range (LR) following topology using the distributed receding horizon control of vehicle platoons. The LR model was tested to monitor the performance indices (stability and string stability), hence it was observed that the platoons suffered from chattering phenomena and slinky effect which are of importance to the optimum performance. Moreover, the communication among the vehicles in the platoons will never be possible on high speed due to the use of sensors on board of limited range; as a result of this, vehicles must be close together before the topology will be effective. Hence the need for an improved topology will cater for the said lapses. The art of topology experienced a remarkable improvement when vehicle following are modeled to be able to communicate using the unidirectional (UD) following [15–17] and the bidirectional (BD) following [16]. Though the vehicles in both the UD and BD are using distributive controllers, in this formation vehicles can only communicate with the immediate vehicle, and by doing that the information on other vehicle in the formation are not known. This leads to unnecessary poor communication and high jerk that affects the performance of the topology, hence an improvement is necessary.

An enhancement was achieved by [16] when bidirectional leader (BDL) following and two predecessor leader (TPL) following were implemented, whereby bidirectional communication between the leader and the follower occurs, and the two followers take orders from the lead vehicle, respectively [18]. The shortcomings of this research work are due to the fact that the formation does not allow any autonomous control of the vehicles but that the vehicles to be only following the lead vehicle. Consequently, any inherent instability in the lead vehicle will be amplified within the string and causes slinky effect and passengers' discomfort. Therefore, the need for improvement in the topologies is necessary.

The most recent topology is the two-look-ahead following by [19, 20], which permits the controlled vehicle to be able to receive information from both the predecessor and the leader. This topology leads to new knowledge in the area of convoy system. Cook and Sudin [20] recorded stable string and acceptable speed with good jerk but the topology does not fully mimic human driving habit, and it uses distributive control, whereby each vehicle has a built-in controller. Hence an improved topology is needed to achieve the full human driving habit and robust convoy that can lead to stable string, comfort and autonomous control of desire vehicle within the convoy.

This chapter introduces vehicle following control using an improved information flow topology (IFT) for vehicle convoy, where the controlling vehicle is expected to be controlled at consensual speed and to maintain desired space with the independent

vehicles, and also to greatly reduce jerk. The proposed following vehicle control topology ensures the information flow from the leader, predecessor and the rear vehicle to the controlled vehicle, where the control vehicle utilizes the information received to adjust in speed and position in the convoy. A dynamic model for the proposed following vehicle is implemented to facilitate realistic, free slinky-effect, high passenger's comfort and safe spacing. The proposed following vehicle would utilize the IFT of the two-vehicle look-ahead plus rear-vehicle and is then compared with the conventional (one-vehicle and two-vehicle look-ahead) convoy to ascertain its dynamic parameters (relative position, speed, acceleration and jerk) performance.

Section 2 of this chapter describes the mathematical modeling of single-vehicle dynamics. The analysis of the proposed following vehicle convoy dynamics model is shown in Sect. 3. Section 4 provides a discussion on the results obtained. Finally, Sect. 5 concludes and gives possible future work.

2 Single-Vehicle External Dynamics

From the Newton's Second Law of Momentum, the acting force can be mathematically expressed as Eq. (1), which is stated as the rate of change in momentum of a body is directly proportional to the applied force in the direction of the applied force [21, 22];

$$\overrightarrow{F} = \frac{d}{dt}\left(m\overrightarrow{v}\right) \tag{1}$$

where $\overrightarrow{F}$ is the force acting on the object at time t in a specific direction, m is the mass of the object and $\overrightarrow{v}$ is the object's speed.

The fundamental law also stands for both translational and rotational motion. In the translational motion, the summation of all external forces acting on the object in a specific direction is equal to the product of its mass and acceleration in the same direction at a fixed mass [23];

$$\sum_{i=1}^{i=\infty} \overrightarrow{F}_{xi} = m\overrightarrow{a}_x \tag{2}$$

where $\overrightarrow{a}_x$ is the acceleration in the forward direction x and $\overrightarrow{F}_{xi}$ is the ith force acting on the object in the same direction as x.

For a vehicle moving in the horizontal direction only, the external forces considered include the aerodynamic drag force, friction drag and the rolling resistance. Equation (3) gives the actual acceleration performance of the vehicle with respect to external disturbances.

$$ma_x = F_x - F_d - F_{fd} - F_{rr} \qquad (3)$$

where F_d is the aerodynamic drag force, F_{fd} is the viscous friction drag force and F_{rr} is the rolling resistance force.

2.1 Aerodynamic Drag

The impact of aerodynamic forces produced on a vehicle comes from two major sources, namely, drag and viscous friction. The aerodynamic drag F_d from air resistance depends on the changes in the squared velocity value of the vehicle (v^2) [24] as given in Eq. (4).

$$F_d \, \alpha \, v^2 \qquad (4)$$

The complete expression for the aerodynamic drag is given in (5) [24–26]:

$$F_d = \frac{1}{2}\left(C_d A \rho_a v^2\right) \qquad (5)$$

where C_d is the non-dimensional drag coefficient, A is the frontal area of the vehicle as shown in Fig. 1 and ρ_a is the density of the ambient air (1.225 kg/m^3).

Equation (5) shows that the aerodynamic drag of a vehicle is determined by the size of the vehicle's frontal area A, while the drag coefficient C_d depends on the vehicle's shape for which the aerodynamic quantity is characterized. The vehicle's frontal area contributes to the effect of the aerodynamic on the vehicle, which can be seen from Eq. (5) [24, 25]. Hence, the aerodynamic drag can also be reduced by decreasing the frontal area of the vehicle where it has direct contact with the wind and also to give shape with easy free airflow [26].

The frontal of each individual car class has been drastically shrunk to its lowest limit according to the Europe car class type [27]. An agreeable formula for an estimate in the vehicle frontal area has been arrived by all manufacturers [27] as in Eq. (6);

$$A \approx 0.81 \times b_t \times h_t \qquad (6)$$

where b_t and h_t are as shown in Fig. 1.

Table 1 presents some values for the frontal area of some selected car classes [25].

Reducing the aerodynamic drag through changes in the vehicle shape is determined experimentally from wind tunnel tests. Its definition comes from (5) as:

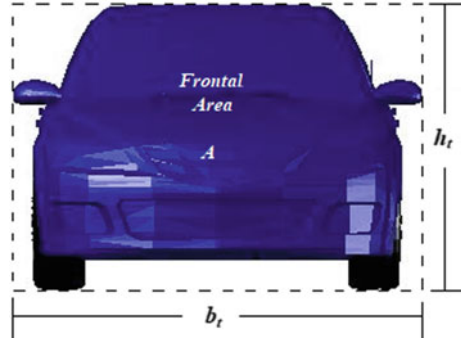**Fig. 1** Definition of the frontal area A of a vehicle

Table 1 Car classification and estimated area

Car class	Mini	Medium size	Upper medium size	Full size
Frontal area A (m^{-2})	1.8	1.9	2.0	2.1

$$C_d = \frac{F_d}{(\frac{1}{2}\rho_a v^2) \times A} \tag{7}$$

where $\frac{1}{2}\rho_a v^2$ is the dynamic pressure.

The drag coefficients of various bodies vary with each other [27, 28]. The typical modern car achieves a drag coefficient of between 0.30 and 0.35 [29]. A four-wheel-drive vehicle, with larger, flatter shape, typically achieves a drag coefficient of between 0.35 and 0.45. Less-powerful engines with the same maximum speed will be obtained from lower F_d [25].

2.2 Viscous Friction Drag

Viscous friction is another form of aerodynamic drag. The viscous friction drag happens when two things (surface of object and airflow) rub together as the object is moving through it. The viscous friction drag can be estimated as in Eq. (7):

$$F_{fd} = \frac{1}{2}(C_{df} \times \rho_f \times b_t \times l \times v^2) \tag{8}$$

where C_{df} is the non-dimensional friction drag coefficient and l is the characteristic length, the chord width of an airfoil.

The friction drag coefficient C_{df} depends on the type of airflow through the vehicle's body. The airflow is defined by the Reynolds number (Re) as in Eq. (9):

Table 2 Classification of friction drag coefficient under three Reynolds number conditions

Type of flow	Laminar flow $(Re < 5 \times 10^5)$	Turbulent flow $(5 \times 10^5 < Re < 10^7)$	Even higher Re $(Re > 10^7)$
C_{df} value	$\frac{2.656}{\sqrt{Re}}$	$\frac{0.148}{\sqrt[5]{Re}}$	$\frac{0.91}{(\log Re)^{2.58}}$

$$Re = \frac{vl}{\upsilon} \tag{9}$$

where υ is the kinematic viscosity that depends on pressure and temperature, which is expressed as in Eq. (10) [25]:

$$\upsilon = \frac{\mu}{\rho_f} \tag{10}$$

For incompressible fluids at standard sea level the values for μ and υ are 1.7894 $\times 10^{-5}$ Nsm^{-2} and 1.4607×10^{-5} m^2 s^{-1}, respectively [25]. The dynamic viscosity of the fluid is represented by μ and ρ_f represents the fluid density.

To simplify our analysis the frictional drag coefficient C_{df} is classified under three conditions of Re, as tabulated in Table 2.

2.3 Rolling Resistance Force

Rolling resistance F_{rr} is the force that acts on the tire while in contact with the surface, which resists the motion of the tire. When the tire moves on the road, it is always deformed at the bottom. The energy spent on such a deformation process on the tire while rolling can be translated into a frictional force, which is called the rolling resistance [30].

The rolling resistance force can be expressed mathematically as in Eq. (11):

$$F_{rr} = C_{rr} \times mg \cos \theta \tag{11}$$

where C_{rr} is the rolling resistance coefficient, g is the acceleration of free fall due to gravity and θ is the slope angle. The typical value for the rolling resistance coefficient is between 0.01 and 0.02 inclusive [31, 32].

2.4 Simplified Vehicle Dynamics

The simplified vehicle dynamic model is used in the simulation of this chapter because it provides an acceptable actual speed as compared with the desired speed [15, 33–35]. In the simplified model, the internal dynamics is represented as a lag function according to Liu et al. [33], in which the vehicle acceleration is obtained after some time delay τ from the given Eq. (12). Liu et al. [33] come up with a value of 0.2 s as τ to represent the vehicle's characteristics of the propulsion systems, which include the engine, transmission, wheels and any other internal controllers.

$$\tau \dot{a} + a = u \tag{12}$$

where τ is the time delay constant, $\dot{a}$ is the vehicle jerk, a is the vehicle acceleration and u is the command signal of acceleration.

Re-arranging Eq. (12) yield expression for the vehicle's jerk as:

$$\dot{a} = \frac{1}{\tau}(u - a) \tag{13}$$

The simplified model of Eq. (13), which considers only the internal dynamics of the vehicle, can be represented by the equivalent block diagram as in Fig. 2.

Next, is to include the effect of external dynamics; the modification will be in Fig. 2 to achieve Fig. 3. By integrating the acceleration performance, the speed and position of the vehicle can be obtained, respectively. Figure 3 gives the representation of the actual acceleration a_{act} performance considered, which is the difference between the acceleration obtained from the vehicle propulsive force a_{pro} and that from the external drag forces a_{dra}. This can be represented mathematically as in Eq. (14):

$$a_{\text{act}} = a_{\text{pro}} - a_{\text{dra}} \tag{14}$$

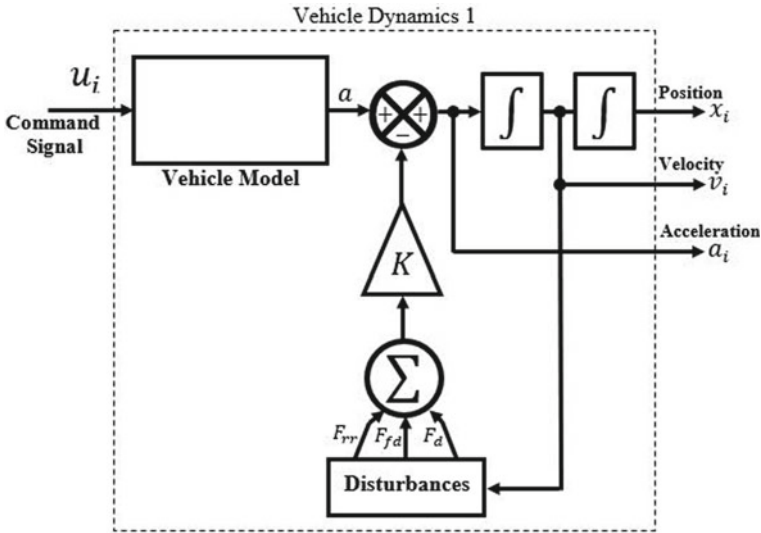**Fig. 2** Simplified vehicle model without external dynamics
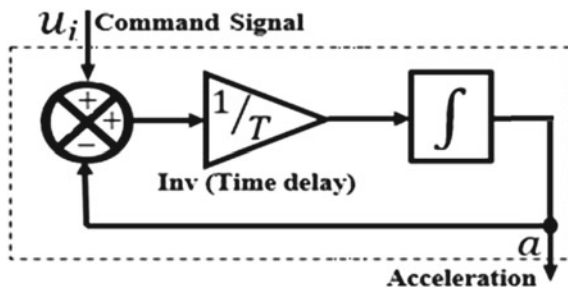
Fig. 3 Overall simplified vehicle dynamics

Reference [25] suggested typical values of a modern vehicle as follows: A is 2.0 m^2, m is 1000 kg, C_{rr} is 0.015, b is 1.4 m and l is 3.0 m for moderate vehicle [25]. These values will be used in the overall simplified vehicle dynamics in Fig. 3 and incorporated into the following vehicle topology.

3 Following Vehicle Convoy Dynamics

In the conventional unidirectional and two-vehicle look-ahead control scenarios, each rigid body mass is assumed to be connected only to its immediate predecessor or two-ahead, respectively. By so doing, the communication range in the conventional vehicle following topology w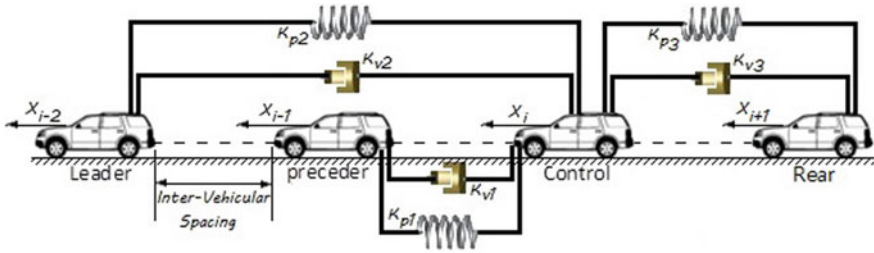ould be limited to only one-vehicle or two-ahead, respectively. This limits the information received by the following vehicle and may lead to chattering, high jerk, passenger's discomfort and unstable string [24].

The proposed topology controls the following vehicle in a convoy using the information of both the preceding vehicle, the vehicle in front of the preceding vehicle and the vehicle at the back of the following vehicle called the rear-vehicle. Figure 4 shows the proposed topology in mass-spring-damper form. The improved convoy operation is considered in a longitudinal dimension where no lane change is permitted. Equation (15) presents the proposed topology derived from Fig. 4 using mass-spring-damper. In the conventional unidirectional and two-vehicle look-ahead control scenarios, each rigid body mass is assumed to be connected only to its immediate predecessor or two-ahead, respectively. By so doing, the communication range in the conventional vehicle following topology would be limited to only one-vehicle

Fig. 4 Representation of the proposed control strategy

or two-ahead, respectively. This limits the information received by the following vehicle and may lead to chattering, high jerk, passenger's discomfort and unstable string [24].

The proposed topology is to control the following vehicle in a convoy using the information of both the preceding vehicle, the vehicle in front of the preceding vehicle and the vehicle at the back of the following vehicle called the rear-vehicle. Figure 4 shows the proposed topology in mass-spring-damper form. The improved convoy operation is considered in a longitudinal dimension where no lane change is permitted. Equation (15) presents the proposed topology derived from Fig. 4 using mass-spring-damper.

$$
\begin{aligned}
m\ddot{x}_i = {} & K_{p1}(x_{i-1} - x_i) + K_{v1}(\dot{x}_{i-1} - \dot{x}_i) + K_{p2}(x_{i-2} - x_i) \\
& + K_{v2}(\dot{x}_{i-2} - \dot{x}_i) + K_{p3}(x_{i+1} - x_i) + K_{v3}(\dot{x}_{i+1} - \dot{x}_i)
\end{aligned}
\tag{15}
$$

The vehicle mass is represented by m, x_i, x_{i-1}, x_{i-2} and x_{i+1} stands for the instantaneous positions of the i, $(i-1)$, $(i-2)$ and $(i+1)$th vehicle, respectively, along the X-axis. $\dot{x}_i$, $\dot{x}_{i-1}$, $\dot{x}_{i-2}$ and $\dot{x}_{i+1}$ are the corresponding velocities of the vehicles, $\ddot{x}_i$ is the acceleration of the ith vehicle, K_{p1}, K_{p2}, K_{p3}, K_{v1}, K_{v2} and K_{v3} are the spring and damper constants, respectively.

The control signal (u_i) has a direct influence on the force applied to the vehicle of mass m [36].

$$
\ddot{x}_i = f(\dot{x}_i, u_i)
\tag{16}
$$

The simplified model can be expressed as in Eq. (17), where u_i is the signal received to accelerate or decelerate the following vehicle. The amount of the controlled vehicle's acceleration is the same as the magnitude of the control signal [36]:

$$
\ddot{x}_i = u_i
\tag{17}
$$

Hence, because the following (ith) vehicle has no influence on the independent vehicles [36] (($i-1$), $(i-2)$ and $(i+1)$th) of the same mass, Eq. (18) is obtained from Eq. (15) as:

$$u_i = K_{p1}(x_{i-1} - x_i) + K_{p2}(x_{i-2} - x_i) + K_{p3}(x_{i+1} - x_i)$$
$$+ K_{v1}(\dot{x}_{i-1} - \dot{x}_i) + K_{v2}(\dot{x}_{i-2} - \dot{x}_i) + K_{v3}(\dot{x}_{i+1} - \dot{x}_i) \qquad (18)$$

Using a fixed spacing policy, the control strategy of the proposed model was presented in Eq. (18). It was evident in [37–41] that the slinky-effect is associated with the fixed spacing policy. Moreover, different inter-vehicular spacing is required for different convoy speed [36]. This is to avoid collision and to give enough time for the controlling vehicle to adjust for sudden changes in the speed of the neighboring vehicles in the convoy. Due to this control challenging problem, a promising policy is necessary; hence the choice of the speed-dependent policy was employed in the proposed model. An improved control signal was achieved by incorporating the constant time headway policy as shown in Eq. (19).

$$u_i = K_{p1}(x_{i-1} - x_i - h\dot{x}_i) + K_{p2}(x_{i-2} - x_i - 2h\dot{x}_i) + K_{p3}(x_{i+1} - x_i - h\dot{x}_i)$$
$$+ K_{v1}(\dot{x}_{i-1} - \dot{x}_i) + K_{v2}(\dot{x}_{i-2} - \dot{x}_i) + K_{v3}(\dot{x}_{i+1} - \dot{x}_i) \qquad (19)$$

The speed-dependent spacing is represented by $h\dot{x}_i$ from Eq. (19). The product of the headway in s and the controlled vehicle's speed are combined to produce displacement, which is inserted in the spring's component as shown in Eq. (19). The product was used in the spring component of the rear and predecessor-vehicle and double of the product was used in the lead-vehicles spring component. The policy used is to create space between the vehicles and to discourage the means of collision. The convoy speed is directly proportional to the vehicle's inter-vehicular spacing [10]. At constant speed, it is assumed that the distance between the leader vehicles (x_{i-2}) and the third (controlling) vehicle (x_i) will be double than that between the fourth (rear) vehicle (t) and the controlling vehicle, or from the second (predecessor) vehicle (x_{i-1}) to the controlling vehicle [10].

Since the following vehicle topology is dependent on the information received from the $(i - 1)$, $(i - 2)$th vehicle look-ahead and the one-rear $(i + 1)$th vehicle, the control signal coming to the controlled vehicle can be re-written from Eq. (19) as [42]:

$$u_i = \sum_{\Psi=1}^{n=2} \left(K_{p\Psi}(x_{i-\Psi} - x_i - \Psi h\dot{x}_i) + K_{v\Psi}(h\dot{x}_{i-\Psi} - \dot{x}_i) \right)$$
$$+ \sum_{\Psi=1} \left(+K_{p3}(x_{i+\Psi} - x_i - \Psi h\dot{x}_i) + K_{v3}(\dot{x}_{i+\Psi} - \dot{x}_i) \right) \qquad (20)$$

For a more compact form, the control signal can be best represented as follows:

$$u_i = \sum_{\Psi=1}^{n=2} \left(K_{p\Psi}(\delta_{im1} - \Psi h\dot{x}_i) + K_{v\Psi}(\dot{x}_{i-\Psi} - \dot{x}_i) \right)$$

$$+ \sum_{\Psi=1} \left(+K_{p3}(\delta_{im2} - \Psi h\dot{x}_i) + K_{v3}(\dot{x}_{i+\Psi} - \dot{x}_i) \right) \tag{21}$$

whereby δ_{im1} and δ_{im2} can be written as the following expressions:

$$\delta_{im1} = \sum_{\Psi=1}^{2} x_{i+\Psi} - x_i - \Psi L \tag{22}$$

$$\delta_{im2} = \sum_{\Psi=1} x_{i+\Psi} - x_i - \Psi L \tag{23}$$

$$\varepsilon_i = x_{i-1} - x_i - L \tag{24}$$

where ε is the inter-vehicular spacing, L is the length of the vehicle including desired spacing. L is the same for each vehicle since the homogeneous type of convoy is assumed, though it may not always be satisfied in practice where the heterogeneous type of vehicle convoy also exists.

Taking the Laplace transform of Eq. (20) gives:

$$S^2 X_i = K_{p1}(X_{i-1} - X_i - hs X_i) + K_{p2}(X_{i-2} - X_i - 2hs X_i) + K_{p3}(X_{i+1} - X_i - hs X_i)$$
$$+ K_{v1}s(X_{i-1} - X_i) + K_{v2}s(X_{i-2} - X_i) + K_{v3}s(X_{i+1} - X_i) \tag{25}$$

Re-arranging for X_i from Eq. (25) gives,

$$X_i = \frac{(K_{v1}s + K_{p1})X_{i-1} + (K_{v2}s + K_{p2})X_{i-2} + (K_{v3}s + K_{p3})X_{i+1}}{s^2 + (K_{v1} + K_{v2} + K_{v3} + (K_{p1} + 2K_{p2} + K_{p3})h)s + K_{p1} + K_{p2} + K_{p3}} \tag{26}$$

Equation (30) gives the reducing form of Eq. (26) to a single-pole system as shown in the following steps:

$$X_i = \frac{K_{v1}\left(s + \frac{K_{p1}}{K_{v1}}\right)X_{i-1} + K_{v2}\left(s + \frac{K_{p2}}{K_{v2}}\right)X_{i-2} + K_{v3}\left(s + \frac{K_{p3}}{K_{v3}}\right)X_{i+1}}{s^2 + (K_{p1} + 2K_{p2} + K_{p3})hs + K_{v1}\left(s + \frac{K_{p1}}{K_{v1}}\right) + K_{v2}\left(s + \frac{K_{p2}}{K_{v2}}\right) + K_{v3}\left(s + \frac{K_{p3}}{K_{v3}}\right)} \tag{27}$$

Hence:

$$X_i = \frac{K_{v1}\left(s + \frac{K_{p1}}{K_{v1}}\right)X_{i-1} + K_{v2}\left(s + \frac{K_{p2}}{K_{v2}}\right)X_{i-2} + K_{v3}\left(s + \frac{K_{p3}}{K_{v3}}\right)X_{i+1}}{s + (s + (K_{p1} + 2K_{p2} + K_{p3})h)s + K_{v1}\left(s + \frac{K_{p1}}{K_{v1}}\right) + K_{v2}\left(s + \frac{K_{p2}}{K_{v2}}\right) + K_{v3}\left(s + \frac{K_{p3}}{K_{v3}}\right)} \tag{28}$$

The pole-zero cancellation technique was used to minimize the complexity of the control law and to guarantee string stability [43]. To achieve a single-pole system (linear equation) Eq. (28) was reduced by incorporating the following constraint:

$$\frac{K_{p1}}{K_{v1}} = \frac{K_{p2}}{K_{v2}} = \frac{K_{p3}}{K_{v3}} = (K_{p1} + 2K_{p2} + K_{p3})h. \tag{29}$$

This results in the simplification of Eqs. (28)–(30) as:

$$X_i = \frac{K_{V1}X_{i-1} + K_{V2}X_{i-2} + K_{V3}X_{i+1}}{s + K_{V1} + K_{V2} + K_{V3}} \tag{30}$$

From Eq. (30) (first-order) it can be seen that K_{v1}–K_{v3} are both positive, which indicates that the poles are to the left-hand side of the s-plane. Hence the proposed mathematical model for the convoy of Eq. (19) is string stable with respect to the constraint of Eq. (29). This implies that the system response of the convoy depends on h and $K_p's$ as seen from Eq. (31).

$$K_{V1} + K_{V2} + K_{V3} = \frac{K_{p1} + K_{p2} + K_{p3}}{(K_{p1} + 2K_{p2} + K_{p3})h} \tag{31}$$

From Eqs. (27) to (31) steps the model was reduced to a single-pole. Eq. (30) could be generalized for an arbitrary number of vehicles ahead and a single rear-vehicle as in Eq. (32) where $k_v = \gamma_v$.

$$X_i = \frac{\gamma_{v3}X_{i+1} + \sum_{m=1}^{n}(\gamma_{vm}X_{i-m})}{s + \sum_{z=1}^{n}\gamma_{zm}} \tag{32}$$

Now the transfer function $G_m(s)$ is given in Eq. (33).

$$G_m(s) = \frac{\sum_{m=1}^{n=3}(K_{vm}s + K_{pm})}{s^2\left(\sum_{\phi=1}^{m=2}\left((K_{v\phi} + \phi h K_{pr})s + K_{p\phi}\right)\right) + \sum_{\phi=3}\left((K_{v\phi} + h K_{p\phi})s + K_{p\phi}\right)} \tag{33}$$

Equation (32) can be greatly simplified by choosing the gain parameters to produce pole-zero cancellations in the transfer function. This can be done by rearranging Eq. (29) for the two-vehicle ahead and rear-vehicle inclusive as follows:

$$\sum_{\phi=1}^{m=3} K_{v\phi} = \frac{1}{h} \tag{34}$$

This simplifies the transfer function Eq. (33) to the form of a simple lag as before:

$$G_m(s) = \frac{K_{vm}}{s + \sum_{\phi=1}^{n=3} K_{v\phi}} \tag{35}$$

Hence, the convoy's string stability can be verified as achieved using the definition in Eq. (36) [20].

$$\rho = \sum_{\phi=1}^{n=3} K_{v\phi} \tag{36}$$

so that:

$$|X_{in}(j\omega)| \leq \frac{\rho}{|\rho + j\omega|} \max_{1 \leq m \leq n} |X_{out}(j\omega)| \tag{37}$$

The expression in Eq. (37) gives attenuation at all frequencies. The requirement of pole-zero cancellation is of course not necessary in principle, but its absence makes the analysis of string stability much more complicated.

4 Turning of Gains and Simulation

Both the model equation with the stated constraints of Eqs. (19) and (29) are used for the simulation of the vehicle following system. The simulation of only the controlled vehicle is presented, which was developed in Simulink as in Fig. 5.

The time headway (h) is set to a unit second, as suggested by Zhao et al. [35]. One h was used between the controlled vehicle and the predecessor or rear, while $2h$ was used between the controlled vehicle and the lead-vehicle due to their distance apart [35]. The constants k_{pn} and k_{vn} where $n = 1, 2$ and 3 are so chosen for stable operation of the control strategy when connected to the vehicle dynamics.

In order to ensure that the pole-zero cancellation of Eq. (26) occurs, which will produce Eq. (30), the appropriate tuning of the gain parameters must be made correctly by complying with Eq. (29). From the control law in Eq. (19), increasing the values of those gains k_p's and k_v's will increase the response of the command signal u_i, to changes in vehicles' position and speed.

Increasing the proportional gains, k_p's will speed up the system response. If the gains (k_p's) were kept increasing, a point will be reached where the system will overshoot the changes. When k_p is increased and k_v is kept constant in Eq. (29), a faster response could be achieved, but high-frequency oscillations are expected as the pole-zero cancellation occurs further away from the origin in s-plane. Increasing the differential gains ($k_v's$) will increase the noise to the system because the differential gains are associated with noise and high-frequency oscillations. When k_v is increased and k_p is kept constant in Eq. (29), the pole-zero cancellation occurs near to the origin of s-plane, which will dominate the system response if the exact cancellation is not
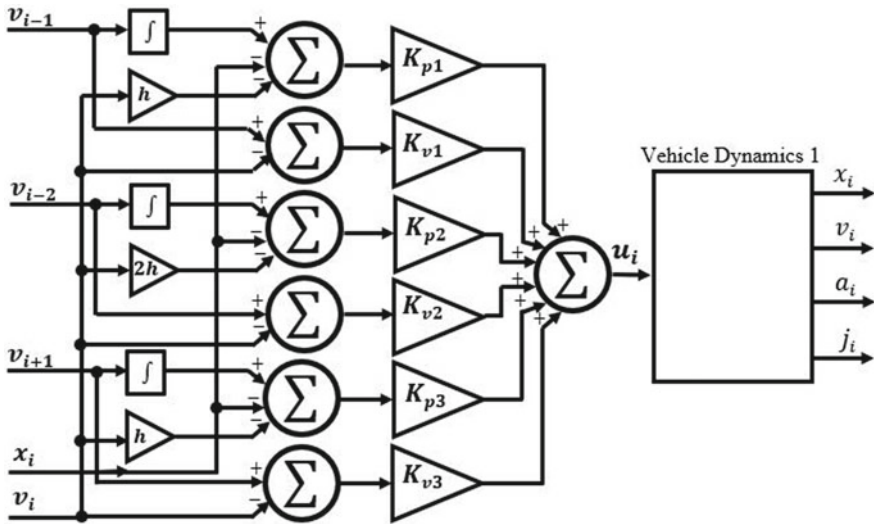
Fig. 5 Simulation model for one vehicle

properly achieved. Therefore, those gains must be kept low in order to avoid the above problems, but the gains must not be too low to prevent a slow response to the system.

Furthermore, it is of importance in this chapter to obtain not only the system control but a balanced response from the controller to changes in both the speed and position of the controlling vehicle. To achieve the said balance response while reducing the measured undesirable effects, the constant k_p is set as equal to k_v for the rear and the respective look-ahead vehicle information, i.e., $k_{v1} = k_{p1}$, $k_{v2} = k_{p2}$ and $k_{v3} = k_{p3}$. The constraints of Eq. (29) give:

$$\frac{K_{p1}}{K_{v1}} = \frac{K_{p2}}{K_{v2}} = \frac{K_{p3}}{K_{v3}} = (K_{p1} + 2K_{p2} + K_{p3})h = 1 \tag{38}$$

In this case, the pole-zero cancellation occurs at $s = -1$ on the s-plane. The speed pattern used in this chapter is a deliberate design that gives the human-driven habit of accelerating, decelerating and maintaining a constant speed.

Several gains were used at Eqs. (39)–(41):

$$\frac{k_p}{k_v} > 1 \tag{39}$$

where gains $k_{p1} = k_{p2} = k_{p2} = 1$; $k_{v1} = k_{v2} = k_{v2} = 0.4$.

$$\frac{k_p}{k_v} \prec 1 \tag{40}$$

with gains $k_{p1} = k_{p2} = k_{p2} = 0.1$; $k_{v1} = k_{v2} = k_{v2} = 0.44$

$$\frac{K_p}{K_v} = 1 \tag{41}$$

where gains $K_{p1} = 0.36$, $K_{p2} = 0.88$, $K_{p3} = 0.053$, $K_{v1} = 0.36$, $K_{v2} = 0.88$ and $K_{v3} = 0.053$.

Hence the need for the correct gains tuning is justified. Rearranging Eq. (38) for each ratio of $K_p \big/ K_v$ yields the following:

$$K_{v1} = \frac{K_{p1}}{\left(K_{p1} + 2K_{p2} + K_{p3}\right)h} \tag{42}$$

$$K_{v2} = \frac{K_{p2}}{\left(K_{p1} + 2K_{p2} + K_{p3}\right)h} \tag{43}$$

$$K_{v3} = \frac{K_{p3}}{\left(K_{p1} + 2K_{p2} + K_{p3}\right)h} \tag{44}$$

Therefore, with $h = 1$ s, k_{p1}, k_{p2} and k_{p3} are so selected to satisfy Eq. (38), while k_{v1}, k_{v2} and k_{v3} are calculated from Eq. (42) to Eq. (44), respectively.

The gains that permit speed changes with the maximum acceleration of fewer than 2 ms^{-2} [44] and the maximum jerk of fewer than 5 ms^{-3} [8] are used. By comparing the gains [Eqs. (39)–(41)], it appears that the appropriate gain among the obtained gains is Eq. (41), hence Eq. (41) is further turned for a satisfactory performance using the gain values of Eq. (45):

$$K_{p1} = 0.11, K_{p2} = 0.38, K_{p3} = 0.13, K_{v1} = 0.11, K_{v2} = 0.38 \text{ and } K_{v3} = 0.13 \tag{45}$$

Figures 6, 7 and 8 show the responses with the gains $K_{p1} = 0.11$, $K_{p2} = 0.38$, $K_{p3} = 0.13$, $K_{v1} = 0.11$, $K_{v2} = 0.38$ and $K_{v3} = 0.13$.

The overall convoy configuration is presented in Fig. 9. The control Eq. (21) and vehicle dynamics Eq. (17) were used in Fig. 9. The overall vehicle convoy is designed and implemented to enable the utilization of human driving habits in the following vehicle. The inter-vehicular spacing together with the vehicle's length is kept at 5 m. The length of a normal car is about 4 m [45–47] which includes the initial spacing.

The headway h is taken to be 1 s [20]. This implies that the spacing of the front of each vehicle to the front of another vehicle is 5 m, assuming all vehicles are initially at rest. The gains k_{vn} and k_{pn} for the control law satisfy the required conditions where the corresponding gains for each vehicle are obtained in Eqs. (42)–(44).
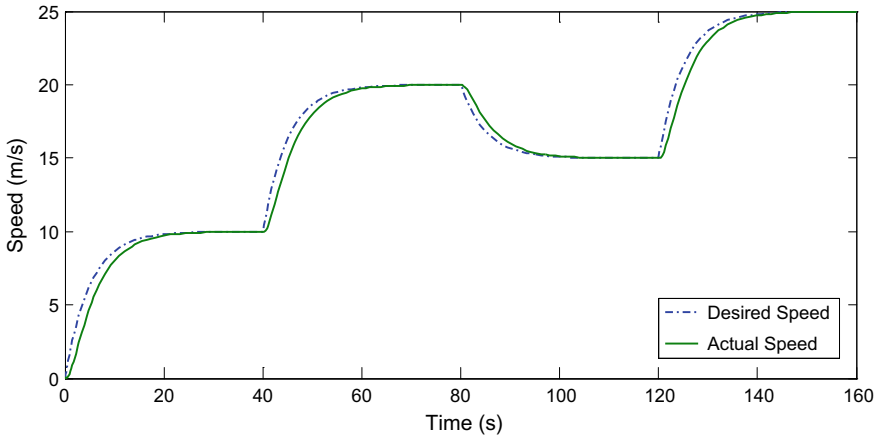
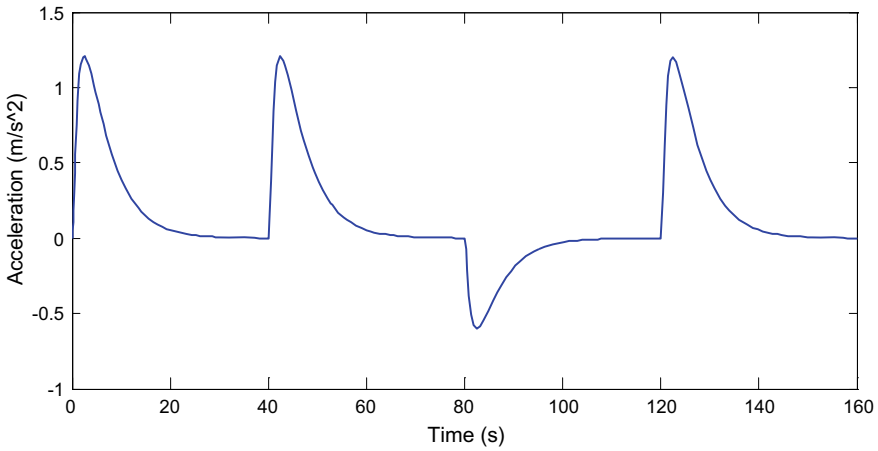**Fig. 6** Speed response of the vehicle when $\frac{K_p}{K_v} = 1$

Fig. 7 Acceleration response of the vehicle when $\frac{K_p}{K_v} = 1$

The model can also be verified by doing a mathematical proof in terms of pole location and pole-zero cancellation under simple classical control theory. From Eq. (25) and substituting the constants obtained in Eq. (45) yields:

$$X_i = \frac{(0.11s + 0.11)X_{i-1} + (0.38s + 0.38)X_{i-2} + (0.13s + 0.13)X_{i+1}}{s^2 + 1.62s + 0.62} \quad (46)$$

Simplifying Eq. (46) gives:
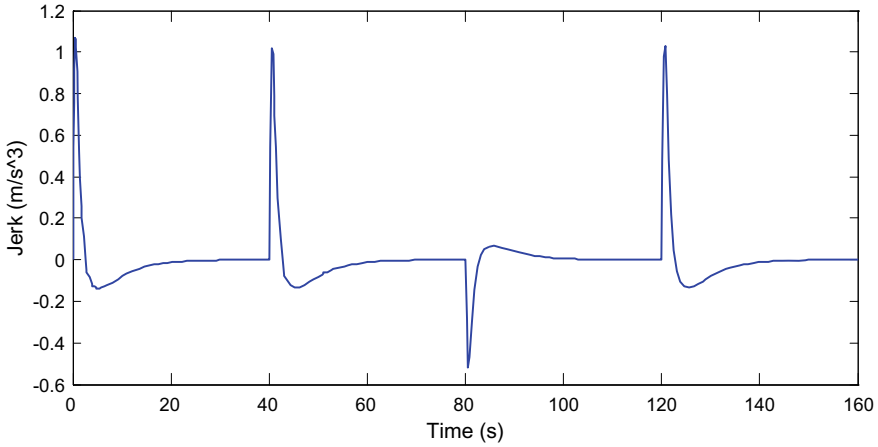
Fig. 8 Jerk response of the vehicle when $\frac{K_p}{K_v} = 1$

$$X_i = \frac{(s+1)(0.11X_{i-1} + 0.38X_{i-2} + 0.13X_{i+1})}{(s+1)(s+0.62)} \tag{47}$$

This shows that the zero at –1 and pole at –1 cancel each other. Hence, leaving only the pole at –0.62 to be the effective pole of the model, that is:

$$X_i = \frac{0.11X_{i-1}}{(s+0.62)} + \frac{0.38X_{i-2}}{(s+0.62)} + \frac{0.13X_{i+1}}{(s+0.62)} \tag{48}$$

In other words, the pole-zero cancellation occurs at $s = -1$ on s-plane and the model has an effective pole at $s = -0.62$ as shown in Figs. 10, 11 and 12.

5 Results and Discussion

The performance of the proposed improved information flow topology can be evaluated through simulation of the topologies' dynamic parameters (position, speed, acceleration and jerk) with a special interest in the following vehicle. The convoy is as designed in Fig. 4, where the following vehicle was controlled by the information (speed and velocity) received from the leading, preceding and the immediate rear-vehicle.

The lead-vehicle starts from rest and gradually rises to a speed of 10 ms^{-1} in 40 s, then accelerate to a velocity of 20 ms^{-1} in 80 s; it then decelerates to 15 ms^{-1} in further 40 s and finally accelerates to a speed of 25 ms^{-1} in 40 s more. The convoy maintains the steady speed trend of changes in velocity over the journey of 160 s with a smooth profile thereafter. The normal convoy operation of a single lane is shown in Figs. 13, 14, 15 and 16.
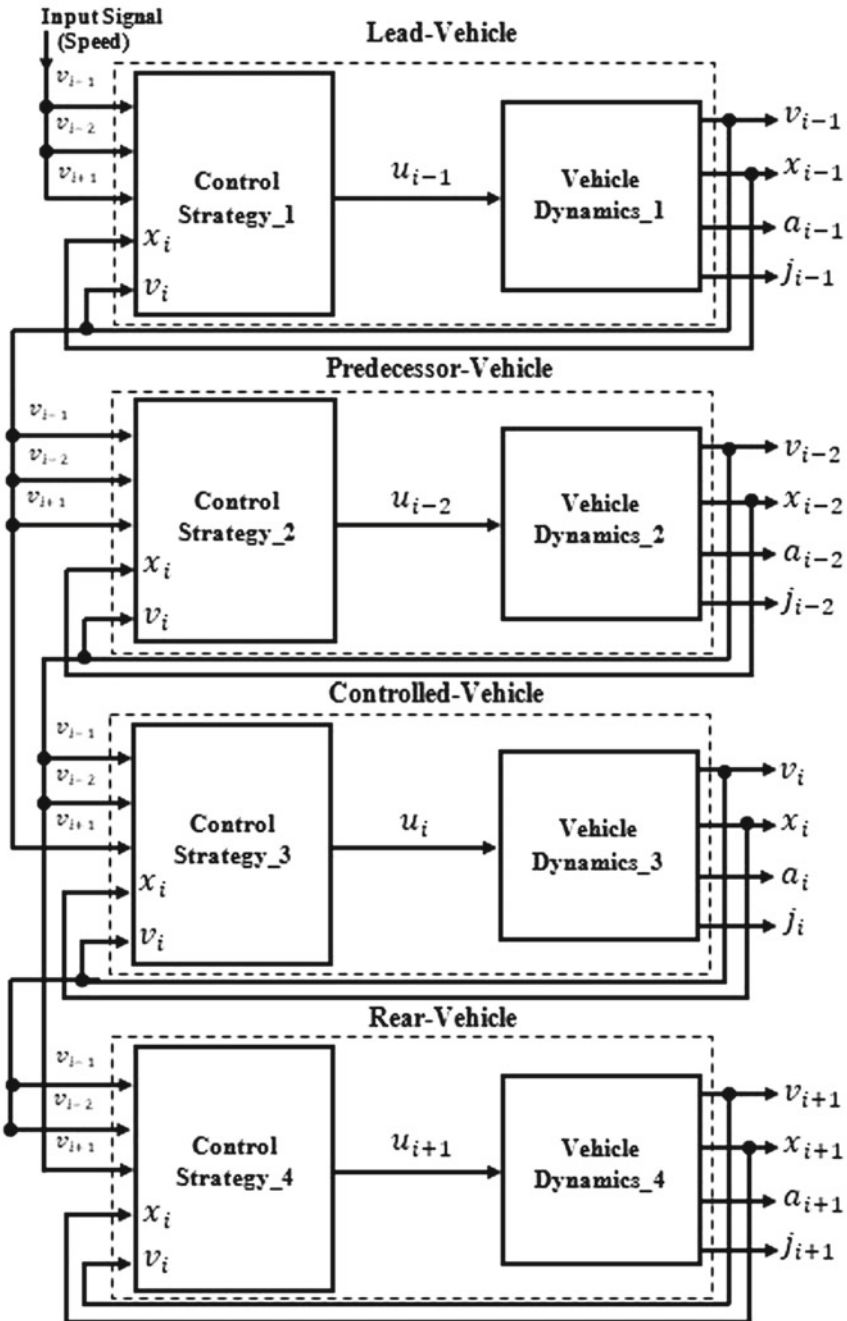
Fig. 9 The overall configuration of the two-ahead and rear-vehicle convoy control
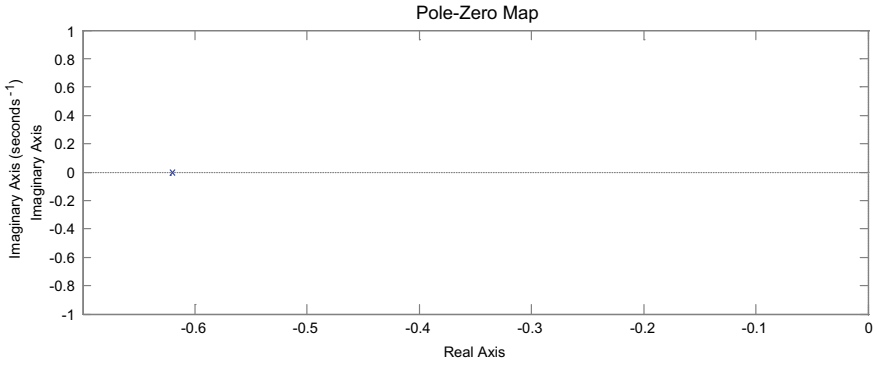
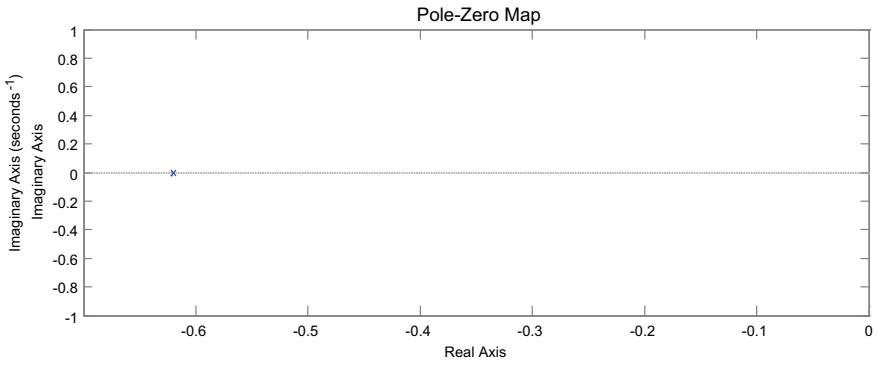**Fig. 10** Poles and zeros location with respect to X_{i-1}

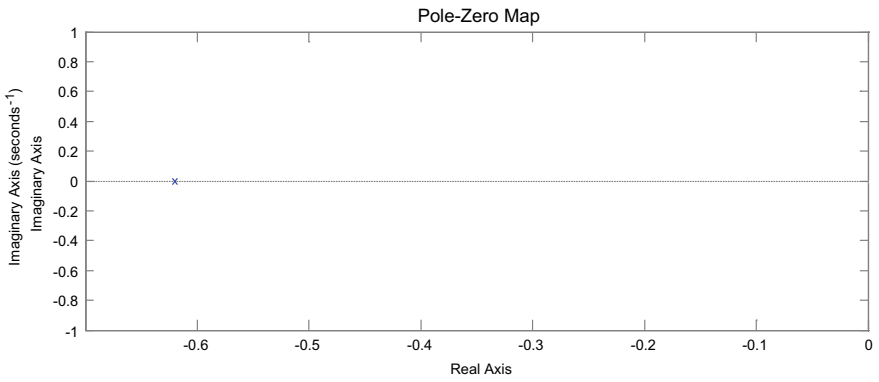**Fig. 11** Poles and zeros location with respect to X_{i-2}

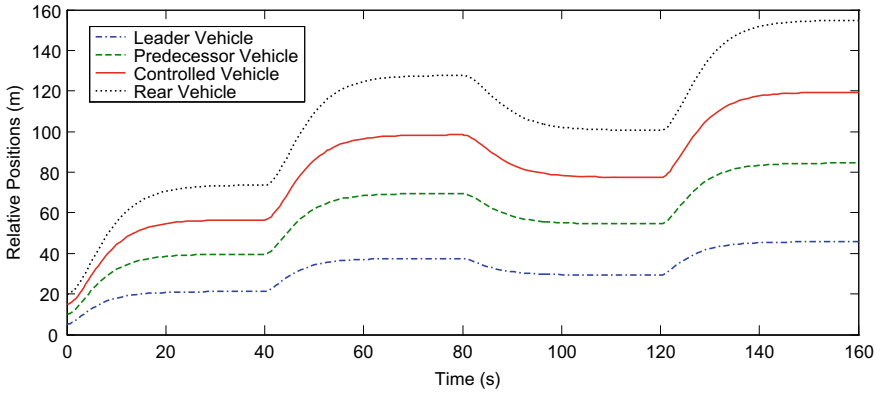**Fig. 12** Poles and zeros location with respect to X_{i+1}

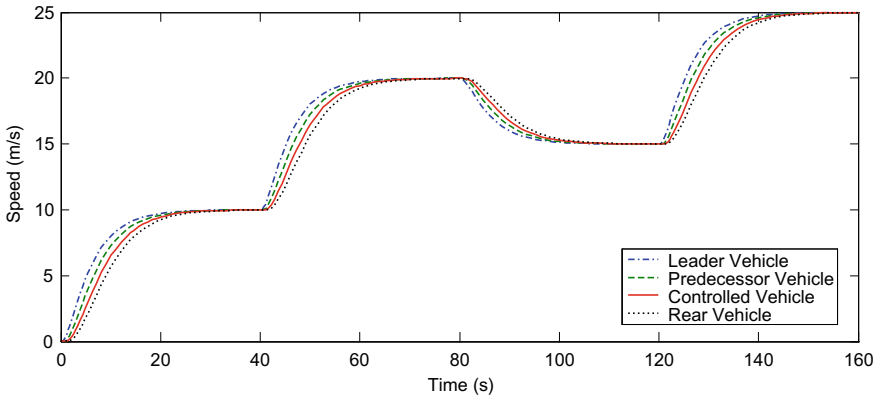**Fig. 13** Relative position of normal convoy operation of the improved topology

Fig. 14 Speed responses of normal convoy operation of the improved topology
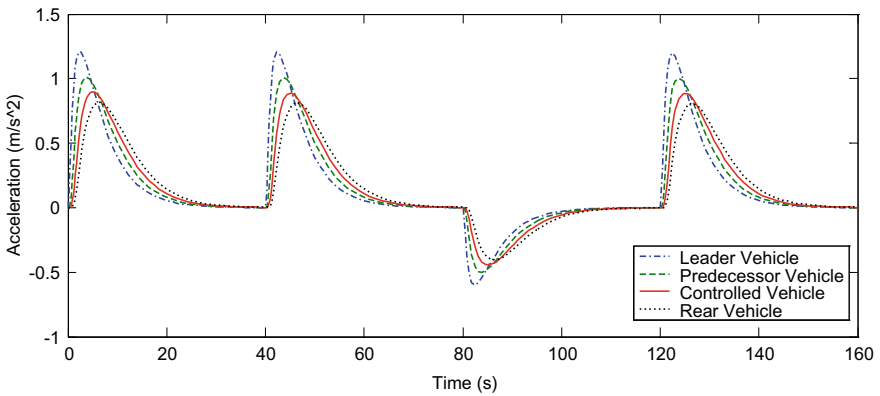

Fig. 15 Acceleration responses of normal convoy operation of the improved topology
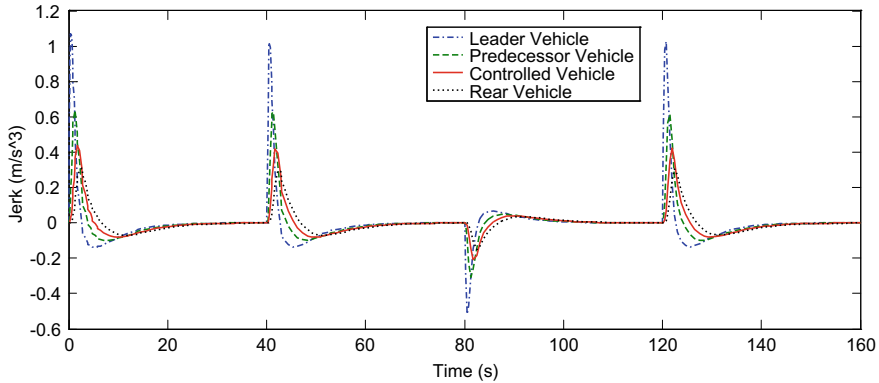
Fig. 16 Jerk responses of normal convoy operation of the improved topology

The convoy moves on the normal operation for the total period of 160 s starting from initial when the time is 0 s. The vehicles in the convoy follow all the changes in the speed of the leading vehicle and maintain close inter-vehicular spacing maneuvers throughout the journey. Figure 13 shows the relative position of each vehicle within the convoy. Figure 13 also shows that the inter-vehicular spacing within the convoy varies according to the convoy's changes in speed while the CTH is set to $h = 1$ s as explained earlier. For instance, at a convoy speed of 10 ms^{-1}, the aggregate inter-vehicular spacing is the combination of the desired spacing of 10 m and the initial set spacing of 5 m gives 15 m. Similarly, at a speed of 20 ms^{-1} the inter-vehicular spacing is 20 m, plus the initial spacing and it continues in this manner.

Figure 14 shows how the control of the proposed topology closely communicates in terms of vehicle speed and tracks the path of leader and predecessor vehicles with much cooperation with the rear-vehicle without collision. This shows the ability of the control vehicle to depend mainly on the acceleration, deceleration and constant speed of the neighboring vehicles.

The improved topology's acceleration was presented in Fig. 15, which shows a smooth and orderly mannered. The controlled vehicle's acceleration was maintained at 0.90 ms^{-2} which is below the maximum acceptable value of 2 ms^{-2} as stated by Rajamani and Shladover [44]. The controlling vehicle's acceleration is adjusted and remains to be between that of the predecessor and the rear-vehicle; this proves proper control of controlled vehicle's acceleration within the convoy.

Among other factors, the passenger's comfort also depends on the vehicle's jerk. The smaller the jerk, the more comfortable the vehicle will be. The jerk of the proposed topology in Fig. 16 is 0.437 ms^{-3}, which is low and far from the maximum rated jerk of 5 ms^{-3} [8, 10]. This value signifies that the control vehicle would be comfortable for passengers [48, 49].

5.1 Comparison of the One-Vehicle Look-Ahead and Two-Vehicle Look-Ahead Against the Proposed Topology

The performance of both the improved topology and conventional (one-look-ahead and two-look-ahead) topologies can be evaluated from the results obtained in Figs. 17, 18, 19, 20, 21, 22, 23, 24, 25, 26, 27 and 28. Both topologies were subjected to similar headway, vehicle profile and time duration of 160 s. Several variations in dynamics parameters were recorded; this is due to the use of ill-topology in the one-look-ahead and the two-look-ahead. Figures 17, 20, 23 and 26 of the one-look-ahead, Figs. 16, 21, 24 and 27 of the two-look-ahead are compared with Figs. 19, 22, 25 and 28 of the improved two-look-ahead and one rear-vehicle convoy topology, respectively, with
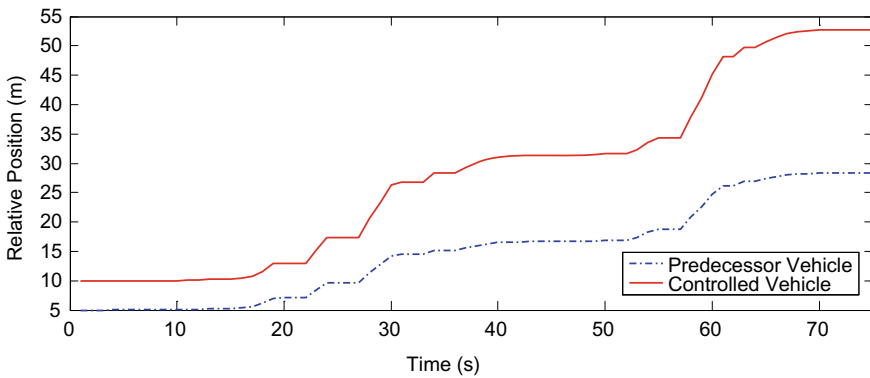

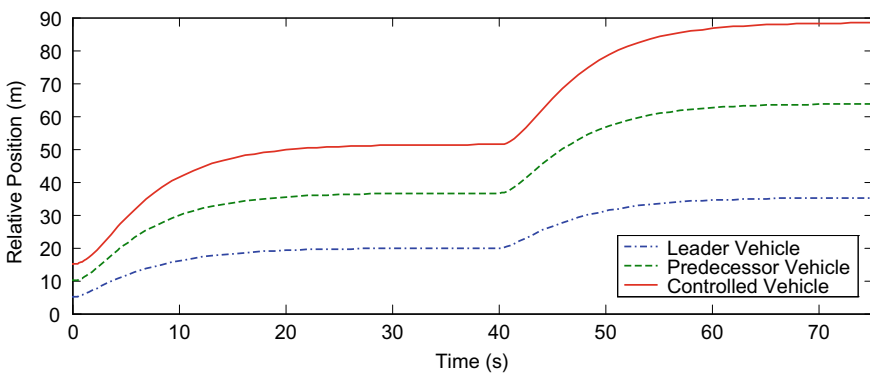**Fig. 17** Relative position responses of one-vehicle look-ahead control topology for *t* equal to 0–75 s

Fig. 18 Relative position responses from the two-vehicle look-ahead control topology for *t* equal to 0–75 s
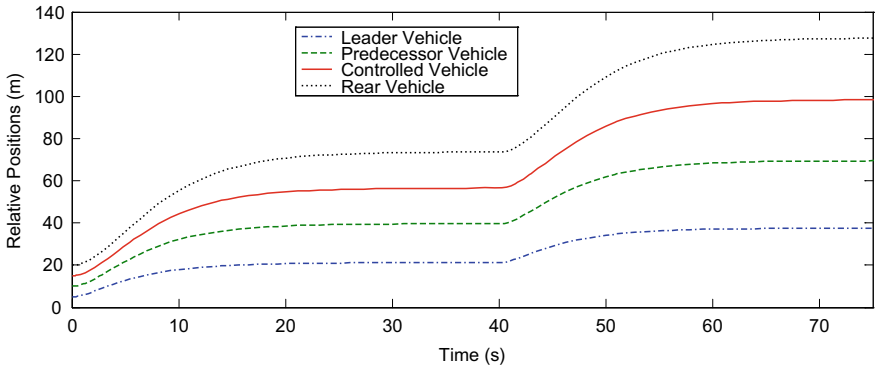
Fig. 19 Relative position responses from the two-vehicle look-ahead and one-rear-vehicle control topology for t equal to 0–75 s
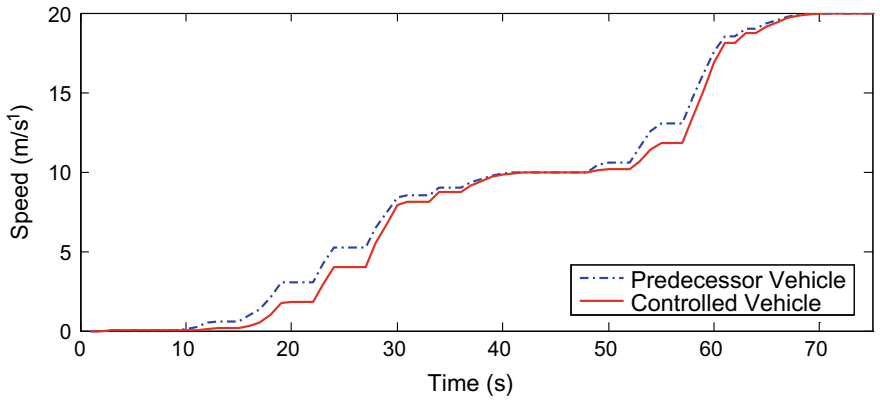

Fig. 20 Speed responses for the one-vehicle look-ahead control topology for t equal to 0–75 s
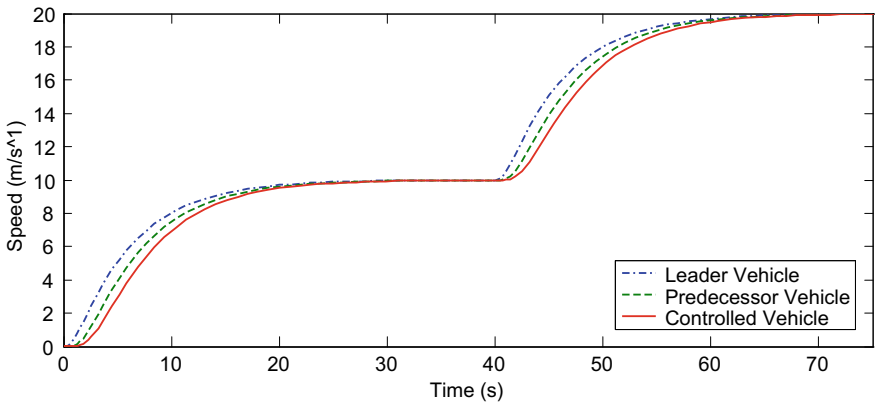

Fig. 21 Speed responses for the two-vehicle look-ahead control topology for t equal to 0–75 s
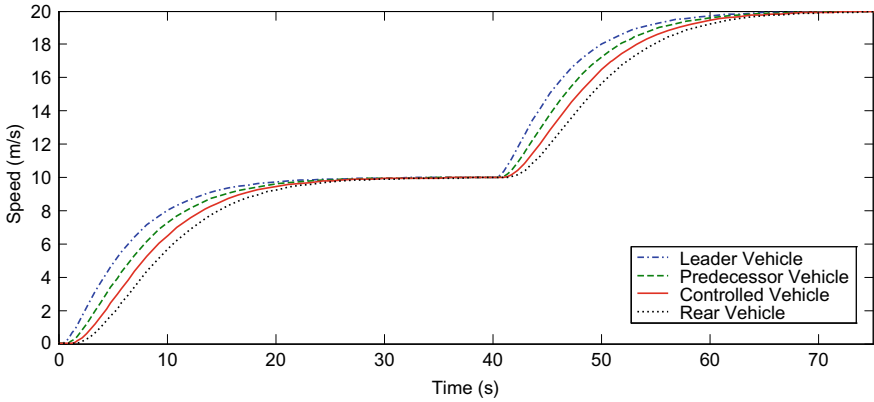
Fig. 22 Speed responses from two-vehicle look-ahead and one-rear-vehicle control topology for *t* equal to 0–75 s
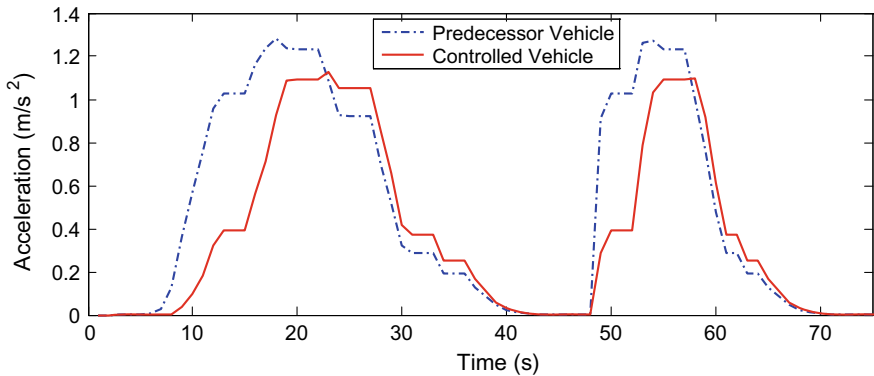

Fig. 23 Acceleration responses from the one-vehicle look-ahead control topology for *t* equal to 0–75 s

both the figures at selected time interest 0–75 s. The selected time interval of 0–75 s is due to the significant changes that occur within the period, which brings about the performance improvement in the topology.

Figure 19 shows the achievement of variable inter-vehicular spacing, as variation in spacing was achieved with respect to variation in the vehicle speed. By implication, for constant speed among the vehicles it will result in an equal inter-vehicular spacing. The inter-vehicular spacing gives an improvement in spacing and slinky free IFT than that of Fig. 17. This improved topology results in a smooth and free running of the vehicle over the test period of 160 s as shown in Fig. 13. Similarly, the policy used in the control-vehicle provides a wider inter-vehicular spacing of 35 m. The achieved wider spacing gives room for the control-vehicle to adjust its speed and position on any sudden changes in speed from the neighboring vehicles within the
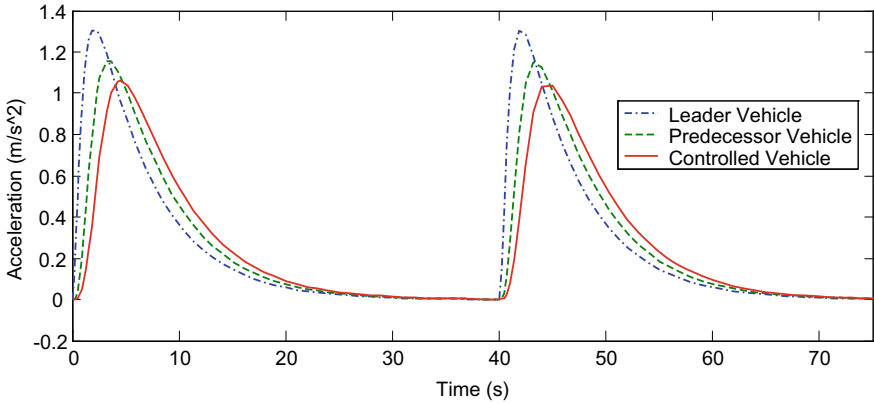
Fig. 24 Acceleration responses from the two-vehicle look-ahead control topology for *t* equal to 0–75 s
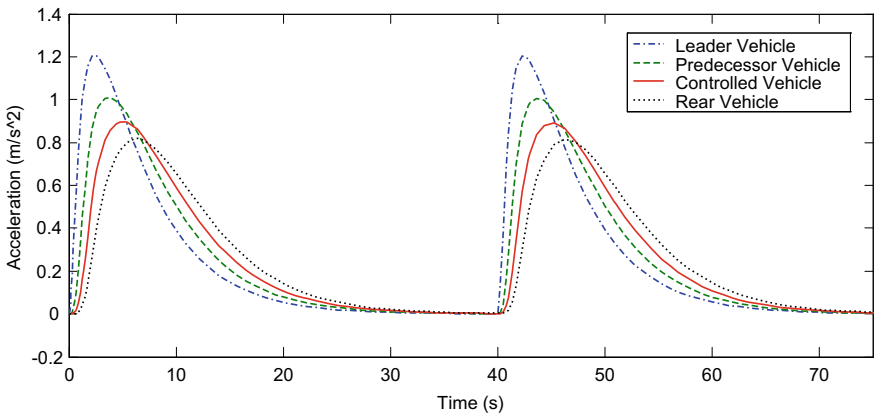

Fig. 25 Acceleration responses for the two-vehicle look-ahead and one-rear-vehicle control topology for *t* equal to 0–75 s

convoy. Figure 17 shows the spacing provided by the improved topology, which avoid collision as the wider spacing will allow the controlling vehicle to take decision due to communication delay.

Shorter inter-vehicular spacing of only 29.3 m was seen in Fig. 17 of the one-vehicle look-ahead topology as compared to the improved topology, even though they are both subjected to similar strategy of CHT. Moreover, chattering was seen for the first 75 s in the spacing provided by the conventional one-look-ahead. Hence, the one-look-ahead is porous to collision on high speed.

Inter-vehicular spacing of 35 m was achieved in the proposed topology as shown in Fig. 19. The improved spacing of the proposed topology is speed-dependent, hence it keeps increasing when the vehicles are on high speed and vice versa. Moreover, the
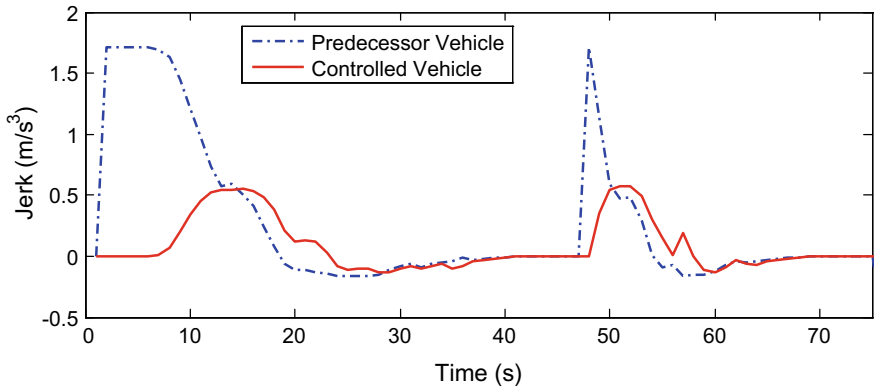
Fig. 26 Jerk responses from the one-vehicle look-ahead control topology for *t* equal to 0–75 s
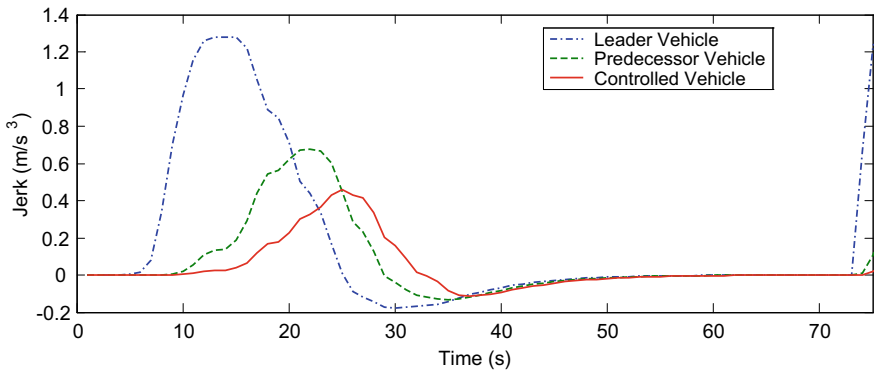

Fig. 27 Jerk responses from the two-vehicle look-ahead control topology for *t* equal to 0–75 s
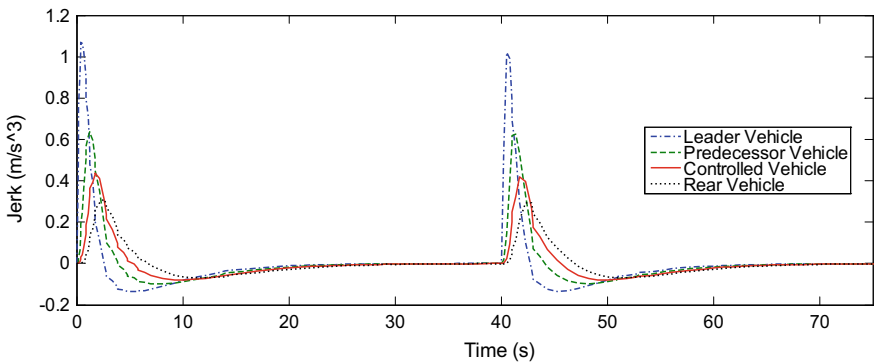

Fig. 28 Jerk responses from the two-vehicle look-ahead and one-rear control topology for *t* equal to 0–75 s

proposed topology gives smooth and free running of the convoy over the set period without overlapping or chattering, as also seen in Fig. 18 for the two-look-ahead topology. The inter-vehicular spacing of Fig. 18 is only 29.61 m, which is lower than that of the improved topology by 5.39 m. The larger inter-vehicular spacing of the proposed topology will avoid collision among and can safely react to sudden changes in the speed of the neighboring vehicles as compared to the two-look-ahead topology.

Figure 22 shows a precise control of the controlled vehicle's speed, who tracks the path of the neighboring vehicles by depending on the information received on their individual speeds without collusion as compared to Figs. 20 and 21 where opposite is the case. Elapses in speed were seen in the one-vehicle look-ahead of Fig. 20. Chattering effect can also be seen in the first 70 s within the journey. The elapses in speed and the chattering resulted in an overlap in speed within the convoy even at low speed of 20 ms^{-1}. This proves that the one-vehicle look-ahead topology is unrealistic.

Figure 22 reveals how the control vehicle of the proposed topology closely tracks the path of the leader, predecessor and rear-vehicle speeds without collusion. The speed of the two-vehicle look-ahead as in Fig. 21 shows an encouraging speed control with similar maneuvering as exhibited in the proposed topology Fig. 22, and all transitions were smooth throughout the journey of 160 s.

The four vehicles acceleration of the improved topology was shown in Fig. 25 within the period of interest of 0–75 s. The controlled vehicle's acceleration was maintained not to pass the threshold value of 0.9 ms^{-2}, which is less than the maximum acceptable value of 2 ms^{-2} [50]. The controlling vehicle's acceleration was adjusted and maintained between the predecessor and the rear-vehicle by using the information received from the neighboring vehicles in the convoy as compared to that of the conventional Fig. 23.

Unwanted oscillation was observed in Fig. 23, and acceleration of 1.129 ms^{-2} was recorded for controlling vehicle of this topology. Though the acceleration is within the acceptable range but it is not as low as that of the proposed topology Fig. 25. The most concern issue of this conventional topology is the chattering phenomena, which occurs at the beginning and last for 75 s. The difference in the acceleration values among the convoys is in favor to the proposed topology by 0.229 ms^{-2}. Hence the improved topology outperformed the one-look-ahead by precise acceleration control of 0.229 ms^{-2} less than that presented in Fig. 23. The less the controlled vehicles' acceleration, the lesser is the jerk.

The acceleration of all the four vehicles in the improved topology was shown in Fig. 25 within the period of interest of 0–75 s. It was found from Fig. 25 that the controlled vehicle's acceleration was maintained not to pass the maximum value of 0.9 ms^{-2}, which is less than the maximum acceptable value of 2 ms^{-2} [50]. The controlling vehicle's acceleration was adjusted and maintained between the predecessor and the rear-vehicle by utilizing the information received from the neighboring vehicles in the convoy. Also, an encouraging result was provided by the two-look-ahead convoy topology, where proper control in acceleration was recorded as well. The two-look-ahead provided an increment in the acceleration of 0.161 ms^{-2} ahead

of the improved topology. This increment in the acceleration of the conventional topologies has consequence on the final controlling vehicle's jerks, which will jeopardize the overall comfortability of the vehicle users. Hence the improved topology outperformed the two-look-ahead by precise acceleration control of 0.161 ms^{-2} less than the one presented in Fig. 24.

To achieve passenger's comfortability, smaller jerk value is required; the smaller the jerk, the more is its comfortability. From Fig. 28 the controlled vehicle's jerk was found to be 0.430 ms^{-3}, which is by far below the maximum required jerk of 5 ms^{-3} [8]. Hence the 0.430 ms^{-3} shows that the controlled vehicle will be comfortable enough for passenger [48, 49] as that of Fig. 26.

Slow response and undesirable jerk of 0.547 ms^{-3} was seen from Fig. 26. The chattering in Fig. 26 indicated the presence of an oscillation as the vehicle is trying to settle to its final speed. The conventional topology of the one-vehicle look-ahead has a higher jerk value as against the proposed topology with 0.144 ms^{-3} difference. This difference in jerk in addition to the oscillation would lead to passenger's discomfort in the conventional convoy.

Similarly, the said jerk of 0.430 ms^{-3} proved to be the set as compared to that of the two-look-ahead as seen in Fig. 27 with a maximum jerk of value of 0.46 ms^{-3}. Moreover, the simulation result of Fig. 27 shows a fast response with minor oscillation at 10–35 s, which was inherited from the acceleration of Fig. 24. This difference in jerk in addition to the short period oscillation would lead to passenger's discomfort in the conventional two-look-ahead convoy topology.

It can be justified by the performance comparison between the improved topology and the conventional one-vehicle look-ahead that the improved topology proved to be of higher performance in terms of all the dynamics parameters.

Table 3 provides a summary of the performance comparison of the improved and the one-vehicle look-ahead convoy topology.

Table 3 Comparison of the improved and one-vehicle look-ahead convoy topology

Dynamics parameters	Position (m)	Speed (ms^{-1})	Acceleration (ms^{-2})	Jerk (ms^{-3})
Proposed	Good spacing of 35 m	Smooth and steady	0.900	0.430
One-vehicle look-ahead	Poor spacing of 29.3 m	Lapses in speed	1.129	0.574

Table 4 Comparison of the improved and two-vehicle look-ahead convoy topology

Dynamics parameters	Position (m)	Acceleration (ms^{-2})	Jerk (ms^{-3})
Proposed	Good spacing of 35 m	0.900	0.43
Two-look-ahead	Acceptable spacing of 29.61 m	1.061	0.46

An improvement of 5.7 m in spacing, smooth and steady speed, 0.229 ms^{-2} in acceleration, 0.144 ms^{-3} in jerk and no chattering phenomena were achieved in proposed improved topology over the conventional one-vehicle look-ahead convoy topology.

It can be justified from the performance comparison between the improved topology and the conventional two-vehicle look-ahead that both the two topologies proved satisfactory spacing, smooth and steady speed, while the improved topology outperforms the two-look-ahead in terms of acceleration and comfort. Table 4 provides a summary of the performance comparison of the improved and the two-vehicle look-ahead convoy topology.

An improvement of 5.39 m in spacing, 0.161 ms^{-2} in acceleration, 0.030 ms^{-3} in jerk and oscillation-free were achieved in the proposed improved topology over the conventional two-vehicle look-ahead convoy topology.

6 Conclusion and Further Work

This chapter aimed to propose vehicle control with improved information flow using two-vehicle look-ahead plus rear-vehicle topology. A resolution was achieved in producing a string stable following vehicle with driving comfort ahead of the conventional. The improved following vehicle can look at one vehicle behind and two vehicles ahead in stable speed and comfort. In conclusion, the improved following vehicle shows that the proposed improved IFT has been designed and implemented. It gave a wider operating range, effective communication and a more realistic vehicle convoy. A control strategy of the improved IFT has been designed and implemented for the following vehicle. Improved results were achieved against the two conventional via simulations since the proposed vehicle topology was string stable and smooth in any changes of vehicle speed due to its potentials in providing acceptable acceleration and rides comfort.

The proposed approach against the one-look-ahead and two-look-ahead achieved the following improvements: An increase in inter-vehicular spacing by 19.45% and 18.20%, respectively; smooth speed, chattering free and ride comfort; a reduction in acceleration by 20.28% and 15.17%, respectively; reduction in jerk by 25.09% and 06.25%, respectively. Hence, it is therefore important to give more emphasis not only on following vehicle convoy but also in the choice of IFT.

The reasons why the proposed topology performs better than the conventional approaches are due to the use of human-like driving habits, variable inter-vehicular

spacing and considering unforeseen circumstances. The human driving habit is the only one that allowed the controlled vehicle to be able to look at the two vehicles ahead of it and the immediate rear vehicle. The proposed topology mimics how human drives by using direct visual to see the two vehicles in front while monitoring the immediate rear vehicle by using the mirrors of the vehicle. By doing so, a stable string was achieved unlike in the conventional topologies whereby only one or two vehicles in front were monitored; hence it leads to unstable string when any of the controlling vehicles suddenly match break. The variable inter-vehicular spacing used in the proposed vehicle topology allowed the controlling vehicle with enough time and space to react to the changes in the speed of the neighboring vehicles for safety. The conventional topologies used constant inter-vehicular which deprived the controlled vehicle with enough time and space to react to any changes in the speed of the neighboring vehicles. Finally, the proposed topology considers the effect of disturbances in terms of frictional force, aerodynamic resistance, rolling resistance and viscous force all in cooperated in the controlled vehicle model as against the conventional that considers only one effect (aerodynamic force). These make the proposed topology performs better than the conventional topologies, which suffered from lack of string stability, exposed to collusion and chattering phenomena.

This chapter opens a way to a new vehicle following control topology that needs to be further explored. Such thematic areas that need to be improved include behavior prediction and adoption, double lane, use of complete vehicle dynamic model and the cooperation of robust controller.

References

1. Rich, T.: 2012 Urban congestion trends operations: the key to reliable travel. U.S. Department of transportation, federal highway administration, US, pp. 1–5 (2013)
2. Lin, S., Zhang, Y., Yu, C., Hu, W., Chen, L., Chang, W.: A DC power-line communication based in-vehicle safety aided system for rear vehicles road safety. In: IEEE 1st Global Conference on Life Sciences and Technologies (LifeTech), pp. 137–138, Osaka, Japan (2019)
3. Ming, L., Haoyu, W., Zhengyu, W., Yifeng, J.: Analysis and warning of corner safety speed of curve based on vehicle structure modeling. In: IEEE 4th Information Technology, Networking, Electronic and Automation Control Conference (ITNEC), pp. 2389–2394, Chongqing, China (2020)
4. Wu, H., Si, Z., Li, Z.: Trajectory tracking control for four-wheel independent drive intelligent vehicle based on model predictive control. IEEE Access **8**, 73071–73081 (2020)
5. Feemster, M.: Using disturbance rejection to achieve inter-vehicle spacing within a convoy. IEEE Trans. Veh. Technol. **68**(6), 5331–5342 (2019)
6. Viel, C., Vautier, U., Wan, J., Jaulin, L.: Platooning control for heterogeneous sailboats based on constant time headway. IEEE Trans. Intell. Transp. Syst. **21**(7), 2078–2089 (2019)
7. Swaroop, D., Shyamprasad, K., Prabhakar, R.P.: Effects of V2V communication on time headway for autonomous vehicles. In: American Control Conference (ACC), pp. 1–14. Seattle, WA, USA (2018)
8. Batra, M., Maitland, A., McPhee, J., Azad, N.L.: Non-linear model predictive anti-jerk cruise control for electric vehicles with slip-based constraints. In: Annual American Control Conference (ACC), pp. 3915–3920, Milwaukee, WI (2018)

9. Turri, V., Kim, Y., Guanetti, J., Johansson, K.H., Borrelli, F.A.: Model predictive controller for non-cooperative eco-platooning. In: American Control Conference (ACC), pp. 2309–2314, Seattle, WA, USA (2017)

10. Musa, M.J., Sudin, S., Mohamed, Z., Nawawi, S.W.: Novel information flow topology for vehicle convoy control. In: Mohamed Ali, M., Wahid, H., Mohd Subha, N., Sahlan, S., Yunus, M., Wahap, A. (eds.) Modeling, Design and Simulation of Systems. Communications in Computer and Information Science, Springer Nature, vol. 751, pp. 323–335, Gateway East, Singapore (2017)

11. Lee, K., Kum, D.: collision avoidance/mitigation system: motion planning of autonomous vehicle via predictive occupancy map. IEEE Access **7**, 52846–52857 (2019)

12. Arogeti, S., Ailon, A.: Formation control and string stability of a group of kinematic vehicles with front-steering wheels. In: 25th Mediterranean Conference on Control and Automation (MED), pp. 1011–1016, Valletta, Malta (2017)

13. Yousef, M., et al.: Dual-mode forward collision avoidance algorithm based on vehicle-to-vehicle (V2V) communication. In: IEEE 61st International Midwest Symposium on Circuits and Systems (MWSCAS), pp. 739–742, Windsor, ON, Canada (2018)

14. Dunbar, W., Caveney, D.: Distributed receding horizon control of vehicle platoons: stability and string stability. IEEE Trans. Autom. Control **57**(3), 620–633 (2012)

15. Khan, M.S., Su, H., Tang, G.: Optimal tracking control of flight trajectory for unmanned aerial vehicles. In: IEEE 27th International Symposium on Industrial Electronics (ISIE), pp. 264–269, Cairns, QLD, Australia (2018)

16. Llatser, I., Festag, A., Fettweis, G.: Vehicular communication performance in convoys of automated vehicles. In: IEEE ICC Ad-hoc and Sensor Networking Symposium, pp. 1–6, Kuala Lumpur, Malaysia. (2016)

17. Ali, A., Garcia, G., Martinet, P.: Safe platooning in the event of communication loss using the flatbed tow truck model. In: IEEE 13th International Conference on Control, Automation, Robotics & Vision, (ICARCV), pp. 1644–1649, Singapore (2014)

18. Tsugawa, S., Kato, S., Aoki, K.: An automated truck platoon for energy saving. In: IEEE/RSJ International Conference on Intelligent Robots and Systems, pp. 4109–4114, San Francisco, CA, USA (2011)

19. Hassan, A.U., Sudin, S.: Road vehicle following control strategy using model reference adaptive control method stability approach. Jurnal Teknologi (Sci. Eng.) **72**(1), 111–117 (2015)

20. Cook, P.A., Sudin, S.: Dynamics of convoy control systems. In: Proceedings of the 10th IEEE Mediterranean Conference on Control and Automation, pp. 9–12. WP7-2. Lisbon, Portugal (2002)

21. Fuse, H., Fujimoto, H.: Fundamental study on driving force control method for independent-four-wheel-drive electric vehicle considering tire slip angle. In: IECON 2018—44th Annual Conference of the IEEE Industrial Electronics Society, pp. 2062–2067, Washington, DC (2018)

22. Musa, M.J., Sudin, S., Mohamed, Z.: Aerodynamic disturbance on vehicle's dynamic parameters. J. Eng. Sci. Technol. School Eng. Taylor's Univ., Malaysia **13**(1), 69–82 (2018)

23. Adam, N.M., Irawan, A.: Steering vehicle with force-based impedance control for inertia reduction. In: IEEE International Conference on Automatic Control and Intelligent Systems (I2CACIS), pp. 47–51, Shah Alam, Malaysia (2018)

24. Huo, Q., Mei, Y.: Study on aerodynamic drag characteristics of high-speed train. In: International Conference on Robots & Intelligent System (ICRIS), pp. 506–509, Changsha, China (2018)

25. Gan, W., Xiang, J., Ma, T., Zhang, Q., Bie, D.: Low drag design of radome for unmanned aerial vehicle. In: IEEE International Conference on Unmanned Systems (ICUS), pp. 18–22, Beijing, China (2017)

26. Muralidharan, V., Balakrishnan, A., Kumar, S.Y.: Design optimization of front and rear aerodynamic wings of a high-performance race car with modified airfoil structure. In: International Conference on Nascent Technologies in the Engineering Field (ICNTE), pp. 1–5, Navi Mumbai (2015)

27. Besselink, B., Johansson, K.H.: String stability and a delay-based spacing policy for vehicle platoons subject to disturbances. IEEE Trans. Autom. Control **62**(9), 4376–4391 (2017)

28. Kandula, J., Kumar, G.S., Bhasker, B.: Experimental analysis on drag coefficient reduction techniques. In: 4th International Symposium on Environmental Friendly Energies and Applications (EFEA), pp. 1–5, Belgrade, Serbia (2016)

29. Travis, W., Bevly, D.M.: Trajectory duplication using relative position information for automated ground vehicle convoys. In: IEEE/ION Position, Location and Navigation Symposium, pp. 1022–1032, Monterey, CA, USA (2008)

30. Trigui, O., Dube, Y., Kelouwani, S., Agbossou, K.: Comparative estimation of electric vehicle rolling resistance coefficient in winter conditions. In: IEEE Vehicle Power and Propulsion Conference (VPPC), pp. 1–6, Hangzhou, China (2016)

31. Seiler, P., Sengupta, R.: Analysis of communication losses in vehicle control problems. In: Proceedings of American Control Conference, IEEE, vol. 2, pp. 1491–1496, Arlington, VA, USA (2001)

32. Swaroop, D., Hedrick, J., Chien, C., Ioannou, P.A.: Comparison of spacing and headway control laws for automatically controlled vehicles. Veh. Syst. Dyn. **23**(1), 597–625 (1994)

33. Liu, K., Gong, J., Kurt, A., Chen, H., Ozguner, U.: Dynamic modeling and control of high-speed automated vehicles for lane change maneuver. IEEE Trans. Intell. Veh. **3**(3), 329–339 (2018)

34. Li, Y., He, C.: Connected autonomous vehicle platoon control considering vehicle dynamic information. In: 37th Chinese Control Conference (CCC), pp. 7834–7839, Wuhan, China (2018)

35. Zhao, Y., Yang, Z., Song, C., Xiong, D.: Vehicle dynamic model-based integrated navigation system for land vehicles. In: 25th Saint Petersburg International Conference on Integrated Navigation Systems (ICINS), pp. 1–4, St. Petersburg, Russia (2018)

36. Kieselbach, R.J.F.: Streamline cars in Germany. In: Aerodynamics in the Construction of Passenger Vehicles 1900–1945. Kohlhammer Ed. Auto and Verk, Stuttgart (1982a)

37. Uhlir, D., Sedlacek, P., Hosek, J.: Practial overview of commercial connected cars systems in Europe. In: 9th International Congress on Ultra-Modern Telecommunications and Control Systems and Workshops (ICUMT), pp. 436–444, Munich, Germany (2017)

38. Nie, G., Hao, Z., Zhao, F., Tian, F.: Fault tolerant control to ensure string stability of cooperative adaptive cruise control under communication interruption. In: IEEE 8th Data Driven Control and Learning Systems Conference (DDCLS), pp. 76–81, Dali, China (2019)

39. Gérard-Philippe, S., Henri, P.G.: Simple algorithms for solving steady-state frictional rolling contact problems in two and three dimensions. Int. J. Solids Struct. Sci. Direct **50**(6), 843–852 (2013)

40. Guo, X., Wang, J., Liao, F., Teo, R.S.H.: Distributed adaptive integrated-sliding-mode controller synthesis for string stability of vehicle platoons. IEEE Trans. Intell. Transp. Syst. **17**(9), 2419–2429 (2016)

41. Trigui, O., Mejri, E., Dube, Y., Kelouwani, S., Agbossou, H.: Energy efficient routing estimation in electric vehicle with online rolling resistance estimation. In: IEEE Vehicle Power and Propulsion Conference (VPPC), pp. 1–6, Belfort, France (2017)

42. Carbaugh, J., Godbole, D. N., Sengupta, R.: Safety and capacity analysis of automated and manual highway systems. In: Transportation Research Part C. Elsevier Science Ltd. UK, vol. 6, nos. 1 & 2), pp. 69–99 (1998)

43. Xie, Q., Filho, C.H.L., Clandfield, F.W., Kar, N.C.: Advanced vehicle dynamic model for EV emulation considering environment conditions. In: IEEE 30th Canadian Conference on Electrical and Computer Engineering (CCECE), pp. 1–4, Windsor, ON, Canada (2017)

44. Rajamani, R., Shladover, S. E.: An experimental comparative study of autonomous and co-operative vehicle-follower control systems. In: Transportation Research Part C. Elsevier Science Ltd. UK, vol. 9, no. 1, pp. 15–31 (2001)

45. Lee, J., Kim, D., Jeong, S., Kim, Y.: Range profile-based vehicle-length estimation using automotive FMCW radar. Electron. Lett. **55**(3), 151–153 (2019)

46. Vrábel, J., Jagelčák, J., Stopka, O., Kiktová, M., Caban, J.: Determination of the maximum permissible cargo length exceeding the articulated vehicle length in order to detect its critical rotation radius. In: XI International Science-Technical Conference Automotive Safety, pp. 1–7, Casta-Papiernicka, Slovakia (2018)
47. Avely, R.P., Wang, Y., Rutherford, G.S.: Length-based vehicle classification using images from uncalibrated video cameras. In: IEEE Intelligent Transportation Systems Conference, pp. 737–742, Washington, DC, WA, USA (2004)
48. Shet, R.A., Schewe, F.: Performance evaluation of cruise controls and their impact on passenger comfort in autonomous vehicle platoons. In: IEEE 89th Vehicular Technology Conference (VTC2019-Spring), pp. 1–7, Kuala Lumpur, Malaysia (2019)
49. Zuska, A., Więckowski, D.: The impact of unbalanced wheels and vehicle speed on driving comfort. In: XI International Science-Technical Conference Automotive Safety, pp. 1–6, Casta-Papiernicka, Slovakia (2018)
50. Zhu, H., Wang, J., Yang, Z.: Numerical analysis on effect of vehicle length on automotive aerodynamic drag. In: IET International Conference on Information Science and Control Engineering (ICISCE2012), pp. 1–4, Shenzhen, China (2012)